

## Article

# Modification of Rare Earth Ce on Inclusions in W350 Non-Oriented Silicon Steel

Haijun Wang<sup>1</sup>, Yuhao Niu<sup>1</sup>, Haitao Ling<sup>1,\*</sup> , Jialong Qiao<sup>1,2</sup> , Yanling Zhang<sup>3</sup>, Wei Zhong<sup>4</sup> and Shengtao Qiu<sup>2</sup>

<sup>1</sup> Anhui Province Key Laboratory of Metallurgical Engineering & Resources Recycling, Anhui University of Technology, Ma'anshan 243002, China

<sup>2</sup> National Engineering Research Center of Continuous Casting Technology, China Iron & Steel Research Institute Group, Beijing 100081, China

<sup>3</sup> State Key Laboratory of Advanced Metallurgy, University of Science and Technology Beijing, Beijing 100083, China

<sup>4</sup> Xinyu Iron and Steel Co., Ltd., Xinyu 338001, China

\* Correspondence: linghaitao@ahut.edu.cn

**Abstract:** In this paper, the effect of rare earth Ce content on the morphology, composition, type and size distribution of inclusions in W350 non-oriented silicon steel was investigated by means of ICP-MS (inductively coupled plasma mass spectrometry), SEM/EDS (scanning electron microscope-energy Dispersive Spectrometer), and ASPEX (automated SEM/EDS inclusion analysis). The results showed that with the increase of Ce content in the steel, the modification sequence of inclusions was  $\text{CeAlO}_3 \rightarrow \text{Ce}_2\text{O}_2\text{S} \rightarrow \text{Ce}_x\text{S}_y$ . The type and size distribution of inclusions in the steel obviously changed with the difference in added Ce content. When the added Ce content in the steel was 10 ppm, 14 ppm, 20 ppm and 30 ppm respectively, the rare earth inclusions were mainly  $\text{CeAlO}_3$ - $\text{Ce}_2\text{O}_2\text{S}$ . Furthermore, when the added Ce content increased to 60 ppm, the rare earth inclusions were mainly  $\text{Ce}_2\text{O}_2\text{S}$  with a small amount of  $\text{CeAlO}_3$  contained in part inclusions. When the added Ce content increased continually to 95 ppm, the rare earth inclusions were mainly  $\text{Ce}_x\text{S}_y$ - $\text{Ce}_2\text{O}_2\text{S}$ . The critical Ce content for the conversion between  $\text{CeAlO}_3$  and  $\text{Ce}_2\text{O}_2\text{S}$  was 41 ppm. To ensure that inclusions transform from  $\text{CeAlO}_3$  to  $\text{Ce}_2\text{O}_2\text{S}$ , the Ce content in the steel should be greater than 41 ppm. Under the current experimental conditions, it was found that when the Ce content was 20 ppm, the number density and proportion of inclusions in the steel were lower, and their average size was larger. When the added Ce content increased to 95 ppm, the number density of inclusions in the steel significantly increased, which deteriorated the steel cleanliness.

**Keywords:** rare earth Ce; inclusions; modification; non-oriented silicon steel; rare earth oxysulfides



**Citation:** Wang, H.; Niu, Y.; Ling, H.; Qiao, J.; Zhang, Y.; Zhong, W.; Qiu, S. Modification of Rare Earth Ce on Inclusions in W350 Non-Oriented Silicon Steel. *Metals* **2023**, *13*, 453. <https://doi.org/10.3390/met13030453>

Academic Editors: Andrii Kostryzhev and Maciej Motyka

Received: 27 December 2022

Revised: 15 February 2023

Accepted: 20 February 2023

Published: 22 February 2023



**Copyright:** © 2023 by the authors. Licensee MDPI, Basel, Switzerland. This article is an open access article distributed under the terms and conditions of the Creative Commons Attribution (CC BY) license (<https://creativecommons.org/licenses/by/4.0/>).

## 1. Introduction

High-grade, non-oriented silicon steel, as the functional material for high-end power equipment [1], is widely applied to the core of large generators and high-efficiency, energy-saving motors and high-efficiency, energy-saving appliances and electric vehicle manufacturing because of its magnetic characteristics of low iron loss and high magnetic induction [2–4]. With the implementation and promotion of frequency conversion technology in the home appliance industry, the rise of the new-energy automobile industry and the development of energy-saving, high-efficiency motors, there is an increasing demand for the magnetic properties of high-grade, non-oriented silicon steel with low iron loss and high magnetic induction [5]. The factors affecting the magnetic properties of high-grade, non-oriented silicon steel are mainly manifested in two aspects: one is the precise control of the composition and cleanliness of the molten steel that is also the basis for determining the magnetic properties of high-grade, non-oriented silicon steel [6]; and the other is a suitable plastic processing and heat treatment process, as there are many micro-sized inclusions in steel which can have adverse effect on the magnetic domain

movement, favorable texture formation and recrystallization process in silicon steel [7]. Rare earth elements have attracted the attention of metallurgical workers much more, because of their unique metallurgical properties. By adding a small amount of rare earth elements into molten steel, the active oxygen and sulfur in the molten steel can be reduced to a lower level, and the microstructure of the finished product can be improved by refining the solidification structure. Meanwhile, rare earth elements can also change the inherent type and morphology of inclusions, reduce the harm of inclusions in experimental molten steel, and improve the related properties of steel products [8–14]. Takashima et al. [15,16] proposed the addition of composite rare earth and Al to non-oriented silicon steel. The results showed that after adding rare earth alloy and Al, the inclusion size became larger, the grain growth rate was significantly improved, the residual stress after annealing was reduced, and the product performance was significantly improved. Wu [17], Liu [18], and Yuan [19] have investigated the application of rare earth elements in non-oriented silicon steel. The research content was mainly based on the addition of pure rare earth elements or rare earth alloy-modified inclusions. Due to their strong deoxidation and desulfurization ability, it was easy to generate rare earth oxides, rare earth sulfides and rare earth oxysulfide compounds by adding appropriate amount of rare earth elements after pre-deoxidation of molten steel. By adding rare earth elements or trace amounts of alloying elements, this could increase the size of inclusions, weaken the pinning effect of original fine inclusions on grain boundaries and magnetic domain walls, make the magnetization process easier, reduce hysteresis loss, and achieve the combination of high magnetic induction and low iron loss. The dispersion precipitation of rare earth elements in molten steel can refine the solidification structure and increase the beneficial texture composition, further improving the magnetic properties of the product. However, it is still unclear whether the mechanism of high melting point phases, such as rare earth oxides (sulfides) as nucleation particles to modify inclusions, can change the type, size and distribution of inclusions in non-oriented silicon steel. Therefore, in this work, efforts have been made to investigate the modification of rare earth Ce on inclusions in W350 non-oriented silicon steel in the laboratory with thermodynamic calculation and experimental analysis, aiming to lay a theoretical foundation for rare earth Ce to modify inclusions in non-oriented silicon steel and provide guidance for production.

## 2. Materials and Methods

The experimental slab of W350 non-oriented silicon steel was produced by a domestic steel company. The slag was removed cleanly before the hot metal entered the desulfurization station, and the slag was removed twice after the deep desulfurization treatment to  $[S] \leq 0.0010\%$ , aiming to minimize the high-sulfur slag entering the converter. The scrap steel required self-produced, high-quality scrap steel, of which about 50% was silicon steel scrap. When the converter was tapping, the slide plate and slag stopper were used to stop the slag, and the thickness of the top slag of the ladle was required to be less than 60 mm. Lime was added to the top slag treatment during the tapping process, and the argon flow rate was controlled during the tapping process to prevent the top slag of the ladle from agglomeration. In the RH refining process, it was forbidden to heat up the molten steel by adding aluminum, after the molten steel had arrived at the RH refining station. After the decarburization, the oxygen content of the molten steel was less than 300 ppm before alloying. Following this, the molten steel was cast into a slab. The raw materials used in the experiment were from the continuous casting slab. The chemical composition of raw materials is listed in Table 1.

**Table 1.** Chemical composition of experimental raw materials (wt.%).

Element	C	Si	Mn	P	S	Als	N
Content	0.0020	2.70	0.32	0.015	0.002	0.50	0.0015

The 150 kg vacuum induction furnace was used for smelting, and the furnace lining was rebuilt before the experiment. The first furnace used pure iron as the raw material to wash the furnace. During the experiment, it was necessary to control the vacuum degree in the furnace, keep the vacuum degree stable; the composition was then adjusted before tapping and rare earth cerium (purity 99.99%) was added, as shown in Table 2. These rare earth cerium alloys were purchased from Beijing Dream Material Technology Co., Ltd. (Beijing, China).

**Table 2.** Chemical composition of rare earth Ce alloy (wt.%).

Element	Fe	Mg	Ni	Si	Ca	C	W	Ce/RE
Content	<0.050	<0.050	<0.050	0.012	0.023	<0.010	0.035	99.9

The steel composition was detected using inductively coupled plasma mass spectrometry (ICP-MS). Table 3 shows the chemical composition of the experimental steel. The rare earth Ce content in 1#~6# experimental steels was 10 ppm, 14 ppm, 20 ppm, 30 ppm, 60 ppm, and 95 ppm, respectively. Samples (20 mm × 15 mm × 15 mm) were taken from the edge of the slab after removing the oxide scale of the slab surface, as shown in Figure 1. After grinding and polishing, the morphology, size and composition of inclusions in the steel were detected and analyzed using automated SEM/EDS inclusion analysis (ASPEX), scanning electron microscope (SEM) and energy dispersive spectrum (EDS) apparatus. The content of total oxygen (T.O.) and nitrogen in the steel were detected by inert gas fusion pulse-infrared absorption spectroscopy.

**Table 3.** Chemical composition of experimental steel (wt.%).

Specimen	C	Si	Mn	P	S	Als	N	O	Ce
1#	0.006	2.65	0.17	0.013	0.002	0.22	0.0017	0.0005	0.0010
2#	0.008	2.30	0.22	0.003	0.002	0.58	0.0018	0.0007	0.0014
3#	0.005	2.67	0.19	0.013	0.002	0.44	0.0020	0.0006	0.0020
4#	0.012	2.30	0.22	0.003	0.002	0.58	0.0020	0.0008	0.0030
5#	0.008	2.71	0.18	0.013	0.002	0.41	0.0025	0.0004	0.0060
6#	0.002	2.31	0.23	0.004	0.002	0.49	0.0025	0.0004	0.0095

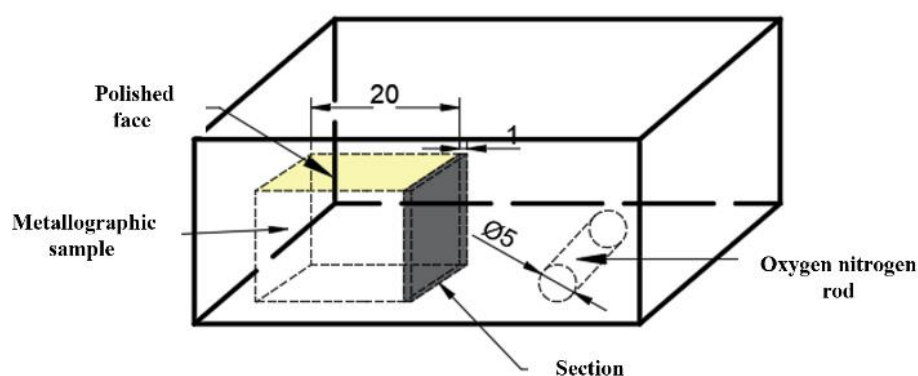


**Figure 1.** Sampling diagram of the experimental steel.

### 3. Results

Figure 2 shows the typical morphology and energy spectrum of inclusions in the steel with 10 ppm Ce content. It can be seen that the type of inclusions in the steel was mainly  $\text{CeAlO}_3\text{-Ce}_2\text{O}_2\text{S-(AlN)}$ , where  $\text{CeAlO}_3\text{-Ce}_2\text{O}_2\text{S}$  are light gray, and AlN in some inclusions was coated with  $\text{CeAlO}_3\text{-Ce}_2\text{O}_2\text{S}$ . The main morphology of  $\text{CeAlO}_3\text{-Ce}_2\text{O}_2\text{S-(AlN)}$  inclusions was spherical or ellipsoidal. The elemental mapping of a typical inclusion is shown in Figure 3.

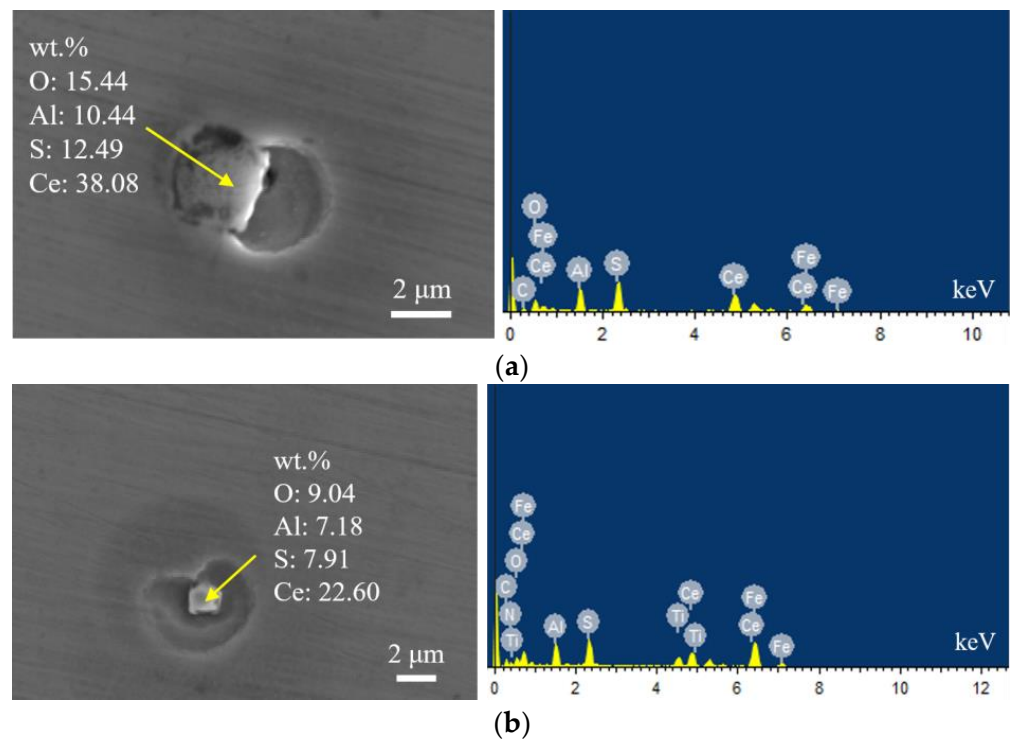


**Figure 2.** Typical morphology and energy spectrum of inclusions in the steel with 10 ppm Ce content. (a) CeAlO<sub>3</sub>-Ce<sub>2</sub>O<sub>2</sub>S, (b) CeAlO<sub>3</sub>-Ce<sub>2</sub>O<sub>2</sub>S.

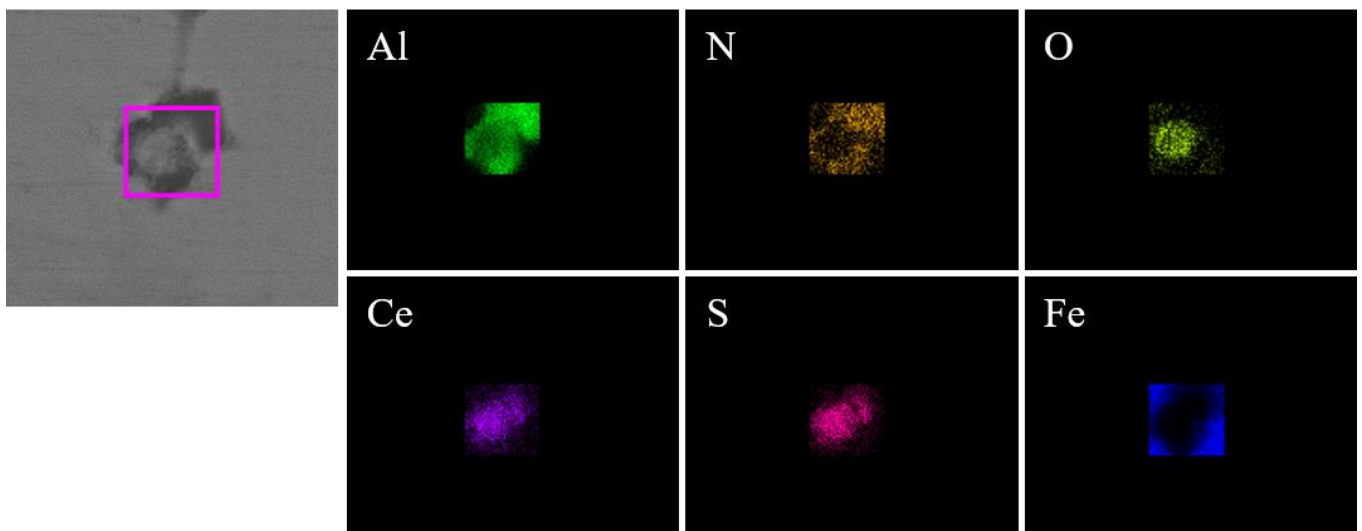


**Figure 3.** Elemental mapping of a typical inclusion in the steel with 10 ppm Ce content.

Figure 4 presents the typical morphology and energy spectrum results of inclusions in the steel with 14 ppm Ce content. The inclusions were composite phases, mainly with CeAlO<sub>3</sub>-Ce<sub>2</sub>O<sub>2</sub>S as the core, and the outer layer was wrapped with AlN. The core of some inclusions was Ce<sub>x</sub>S<sub>y</sub>-CeAlO<sub>3</sub> and its morphology was spherical. The outer layer was wrapped with sharp-angled Al<sub>2</sub>O<sub>3</sub>-SiO<sub>2</sub>. The elemental mapping of a typical inclusion is shown in Figure 5.

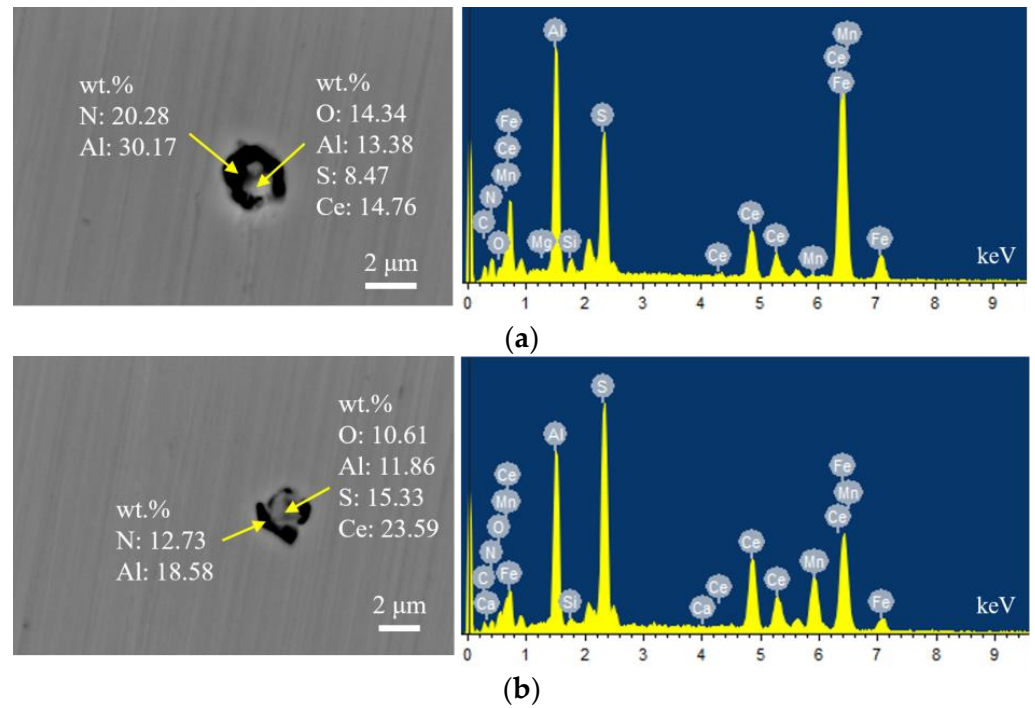


**Figure 4.** Typical morphology and energy spectrum of inclusions in the steel with 14 ppm Ce content. (a) Inner layer:  $\text{CeAlO}_3\text{-Ce}_2\text{O}_2\text{S}$ , Outer layer:  $\text{AlN}$ , (b) Inner layer:  $\text{CeAlO}_3\text{-Ce}_2\text{O}_2\text{S}$ , Outer layer:  $\text{AlN}$ .

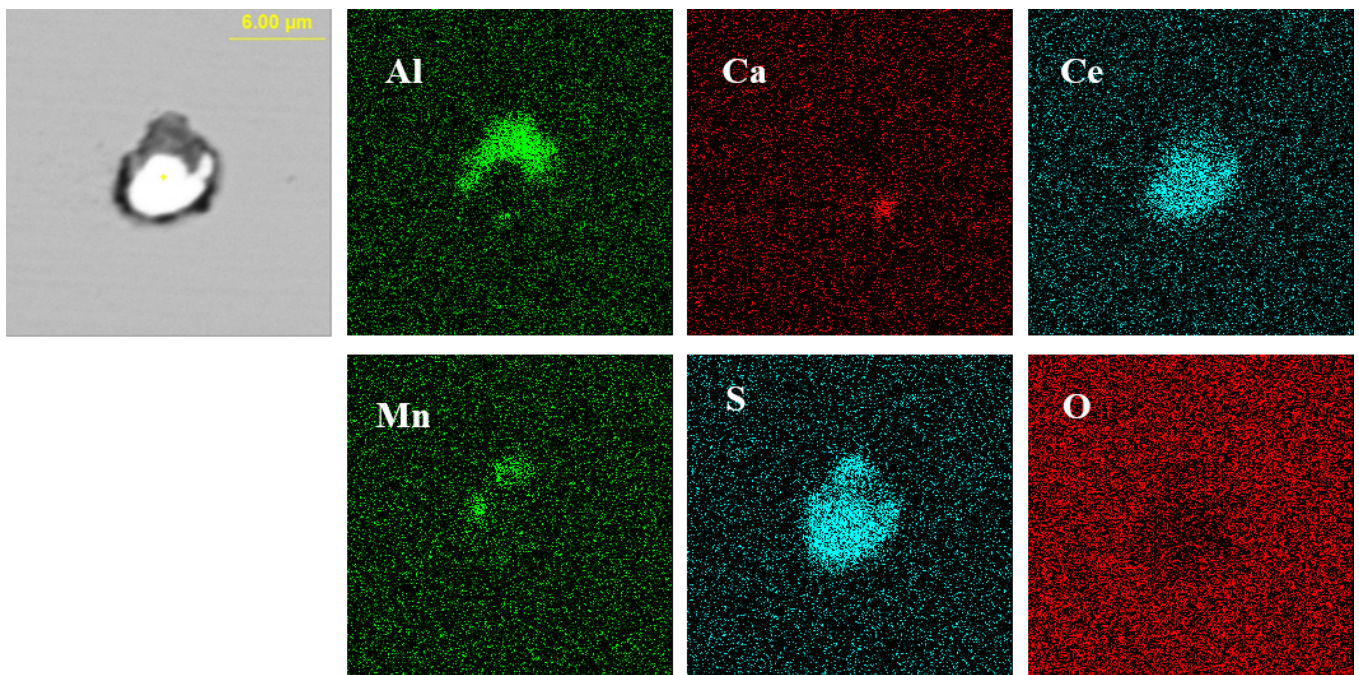


**Figure 5.** Elemental mapping of a typical inclusion in the steel with 14 ppm Ce content.

Figure 6 shows the typical morphology and energy spectrum results of inclusions in the steel with 20 ppm Ce content. The inclusions in the steel were mainly composite phases, with  $\text{CeAlO}_3\text{-Ce}_2\text{O}_2\text{S}$  as the core. The morphology of inclusions was spherical or ellipsoidal, and the outer layer was wrapped with  $\text{AlN}$ . The elemental mapping of a typical inclusion is shown in Figure 7.

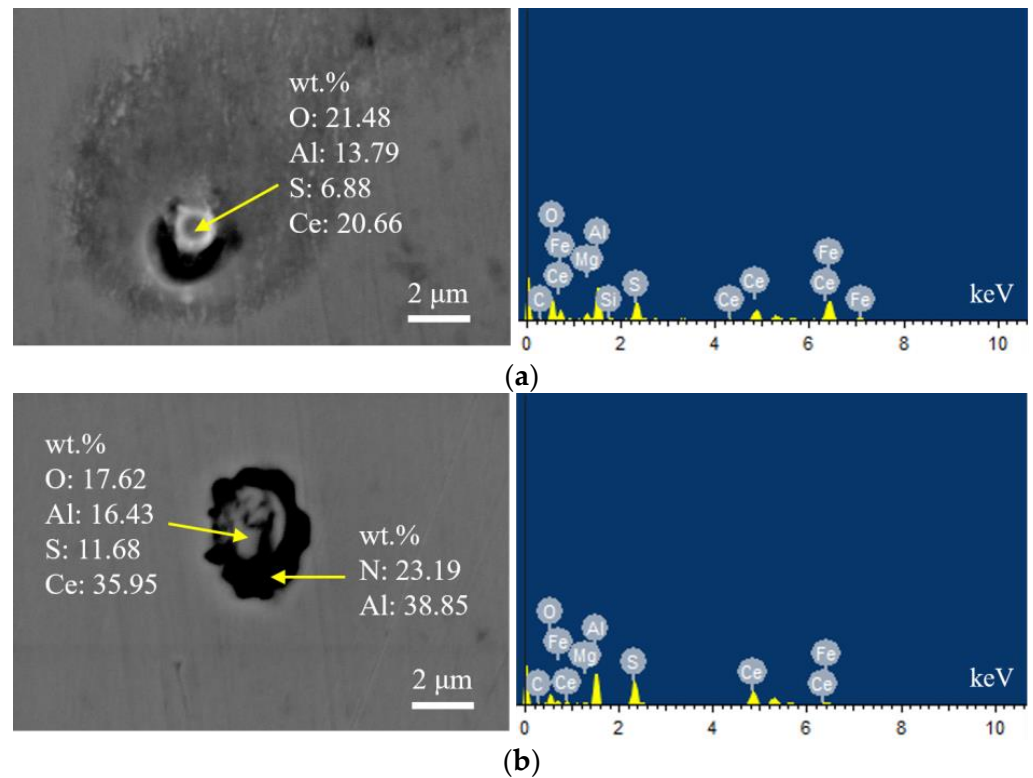


**Figure 6.** Typical morphology and energy spectrum of inclusions in the steel with 20 ppm Ce content. (a) CeAlO<sub>3</sub>-Ce<sub>2</sub>O<sub>2</sub>S, (b) Inner layer: CeAlO<sub>3</sub>-Ce<sub>2</sub>O<sub>2</sub>S, Outer layer: AlN.

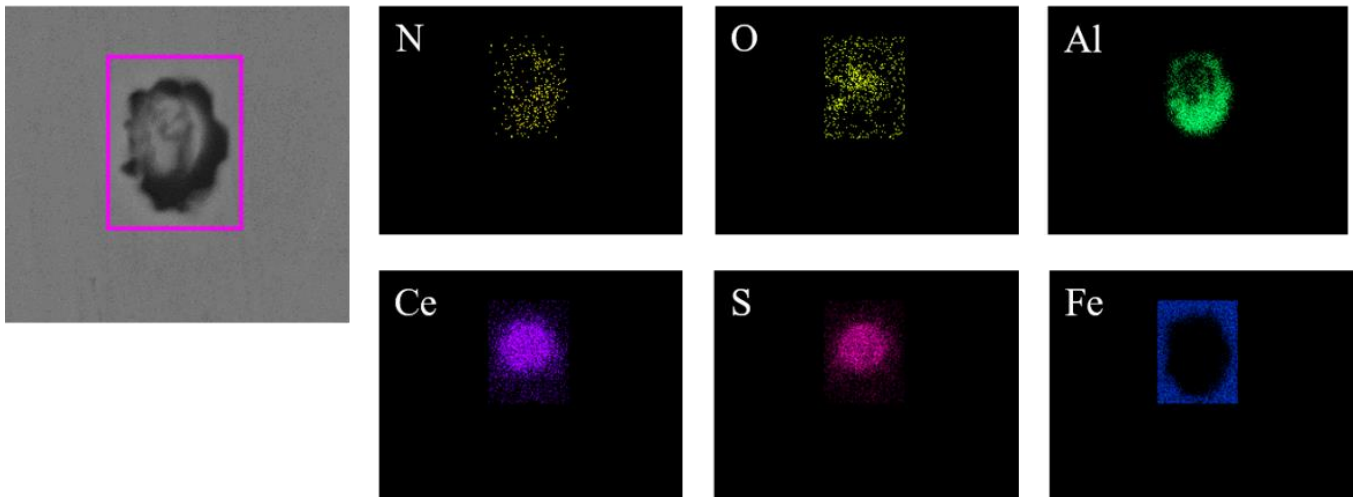


**Figure 7.** Elemental mapping of a typical inclusion in the steel with 20 ppm Ce content.

Figure 8 shows the typical morphology and energy spectrum results of inclusions in the steel with 30 ppm Ce content. It can be seen that the main types of inclusions in the steel were CeAlO<sub>3</sub>-Ce<sub>2</sub>O<sub>2</sub>S-AlN. The inner layer was wrapped with CeAlO<sub>3</sub>-Ce<sub>2</sub>O<sub>2</sub>S and its morphology was spherical. The outer layer was wrapped with irregularly shaped AlN. The elemental mapping of a typical inclusion is shown in Figure 9.

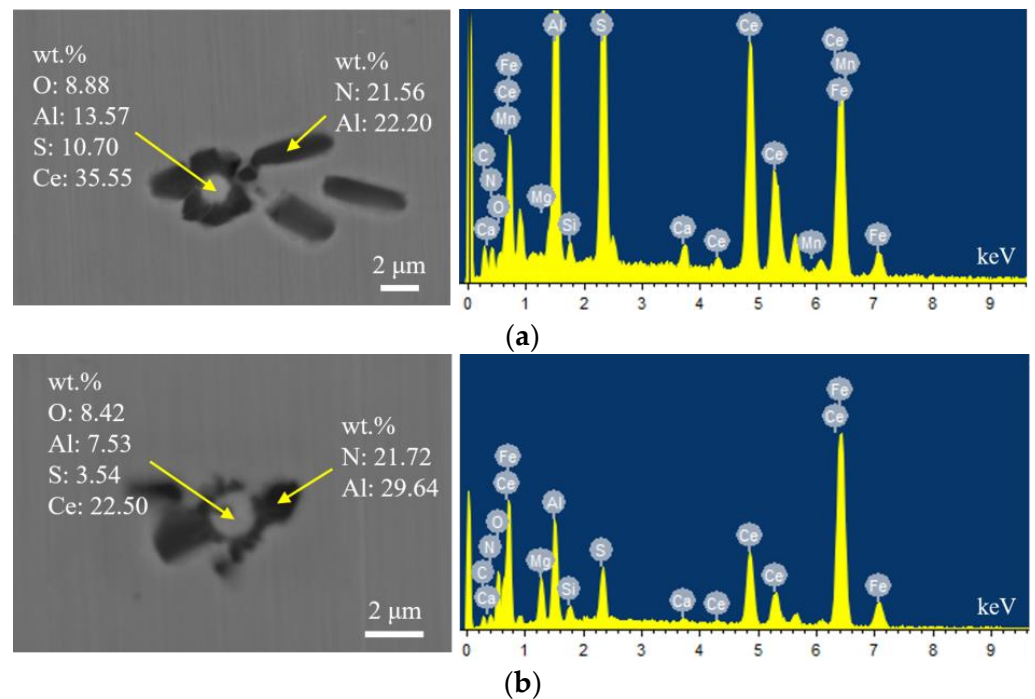


**Figure 8.** Typical morphology and energy spectrum of inclusions in the steel with 30 ppm Ce content. (a) Inner layer:  $\text{CeAlO}_3\text{-Ce}_2\text{O}_2\text{S}$ , Outer layer:  $\text{AlN}$ , (b) Inner layer:  $\text{CeAlO}_3\text{-Ce}_2\text{O}_2\text{S}$ , Outer layer:  $\text{AlN}$ .

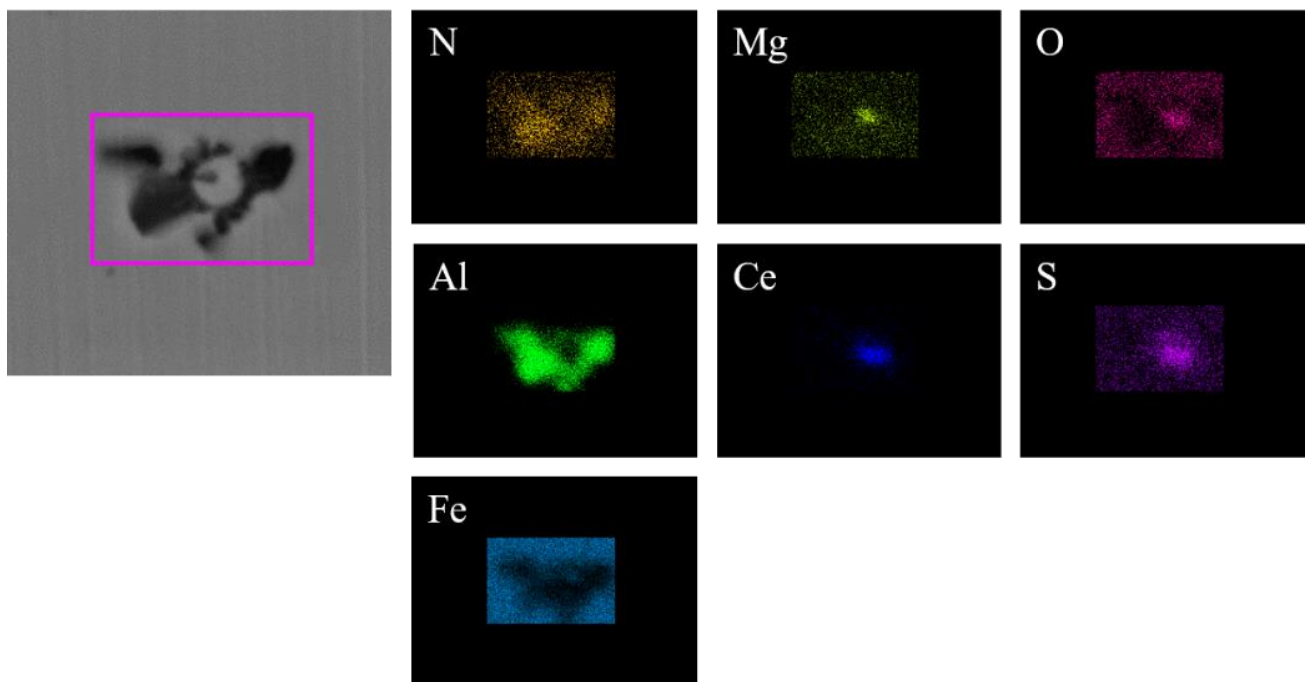


**Figure 9.** Elemental mapping of a typical inclusion in the steel with 30 ppm Ce content.

Figure 10 shows the typical morphology and energy spectrum results of inclusions in the steel with 60 ppm Ce content. It was found that when the Ce content increased to 60 ppm, the types of inclusions in the steel were mainly  $\text{CeAlO}_3\text{-Ce}_2\text{O}_2\text{S-AlN}$  and  $\text{Ce}_2\text{O}_2\text{S-AlN}$ . The morphology of  $\text{Ce}_2\text{O}_2\text{S}$  inclusions was approximately spherical. As shown in Figure 11, the core of the inclusion was  $\text{Ce}_x\text{S}_y\text{-Ce}_2\text{O}_2\text{S}$  and the outer layer was wrapped with  $\text{MgO}\cdot\text{Al}_2\text{O}_3$  phase.

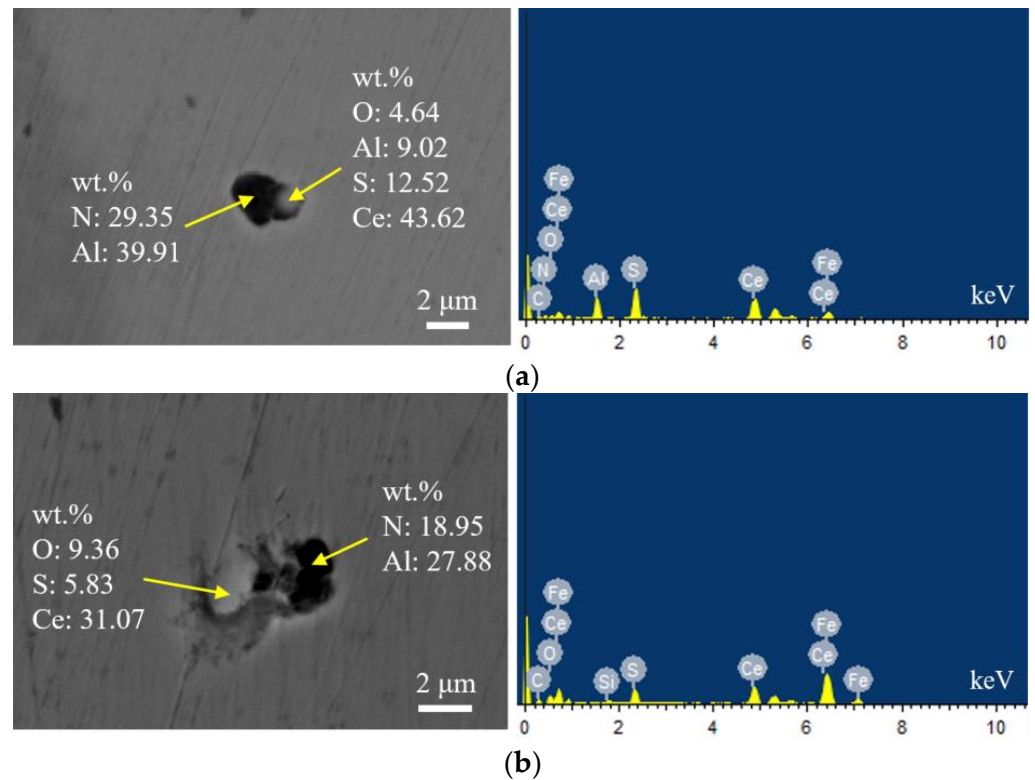


**Figure 10.** Typical morphology and energy spectrum of inclusions in the steel with 60 ppm Ce content. (a)  $\text{CeAlO}_3\text{-Ce}_2\text{O}_2\text{S-AlN}$ , (b)  $\text{Ce}_2\text{O}_2\text{S-AlN}$ .

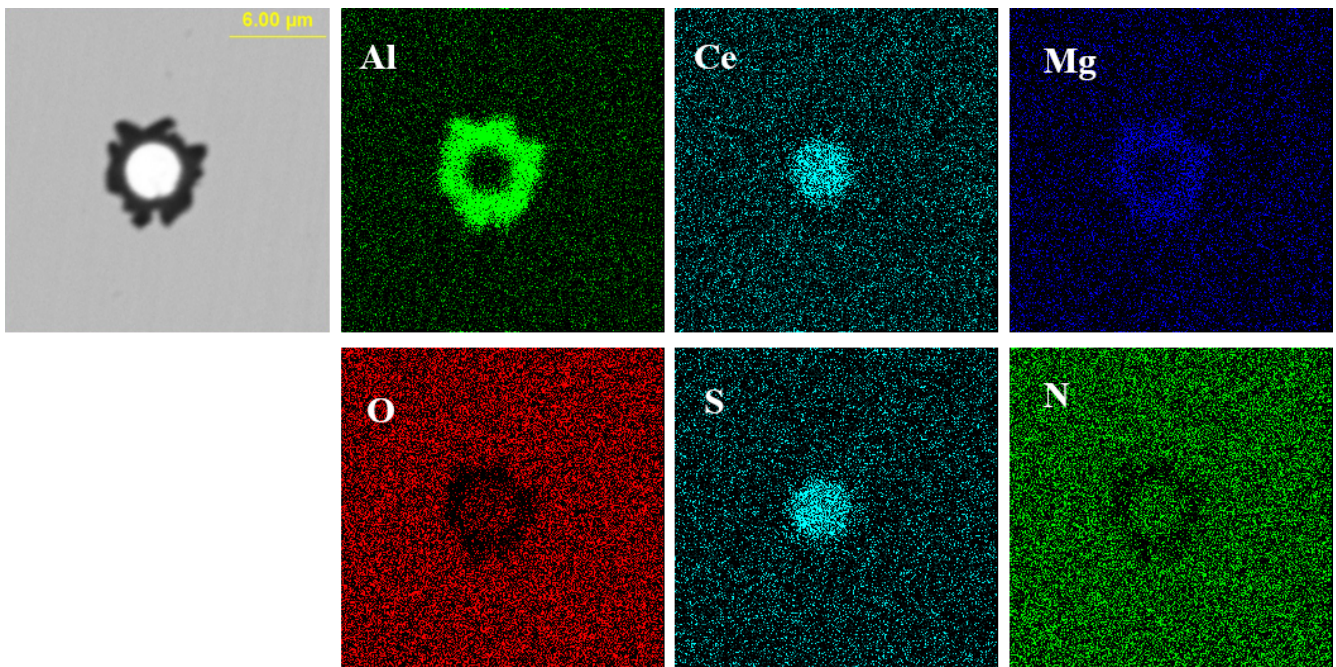


**Figure 11.** Elemental mapping of a typical inclusion in the steel with 60 ppm Ce content.

Figure 12 presents the typical morphology and composition of inclusions in the steel with 95 ppm Ce content. When the Ce content increased to 95 ppm, the core of inclusions in the steel was  $\text{Ce}_x\text{S}_y\text{-Ce}_2\text{O}_2\text{S}$  and its morphology was spherical or ellipsoidal. The outer layer of some inclusions was wrapped with AlN or  $\text{MgO}\cdot\text{Al}_2\text{O}_3$  phase. The elemental mapping of a typical inclusion is shown in Figure 13.

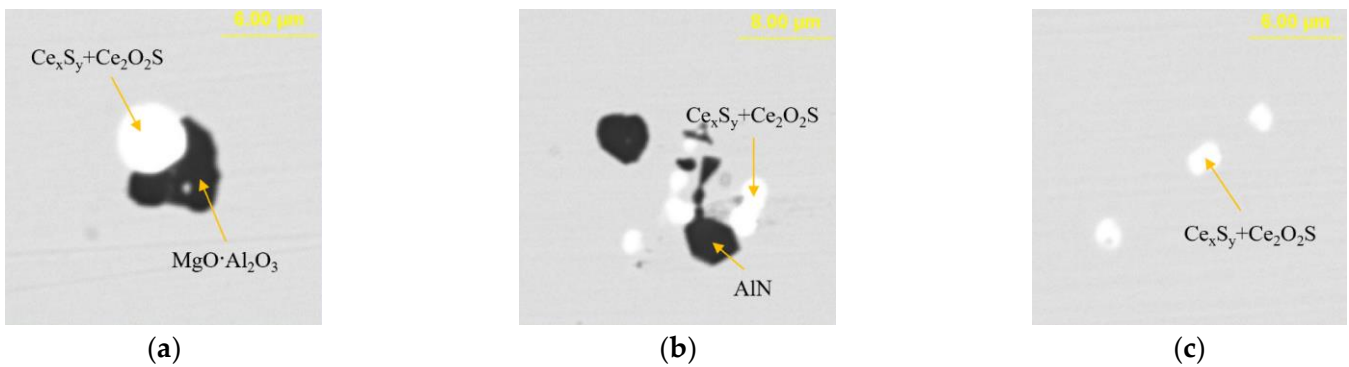


**Figure 12.** Typical morphology and energy spectrum of inclusions in the steel with 95 ppm Ce content. (a)  $Ce_xS_y-Ce_2O_2S-MgO \cdot Al_2O_3$ , (b)  $Ce_xS_y-Ce_2O_2S-AlN$ , (c)  $Ce_xS_y-Ce_2O_2S$ .

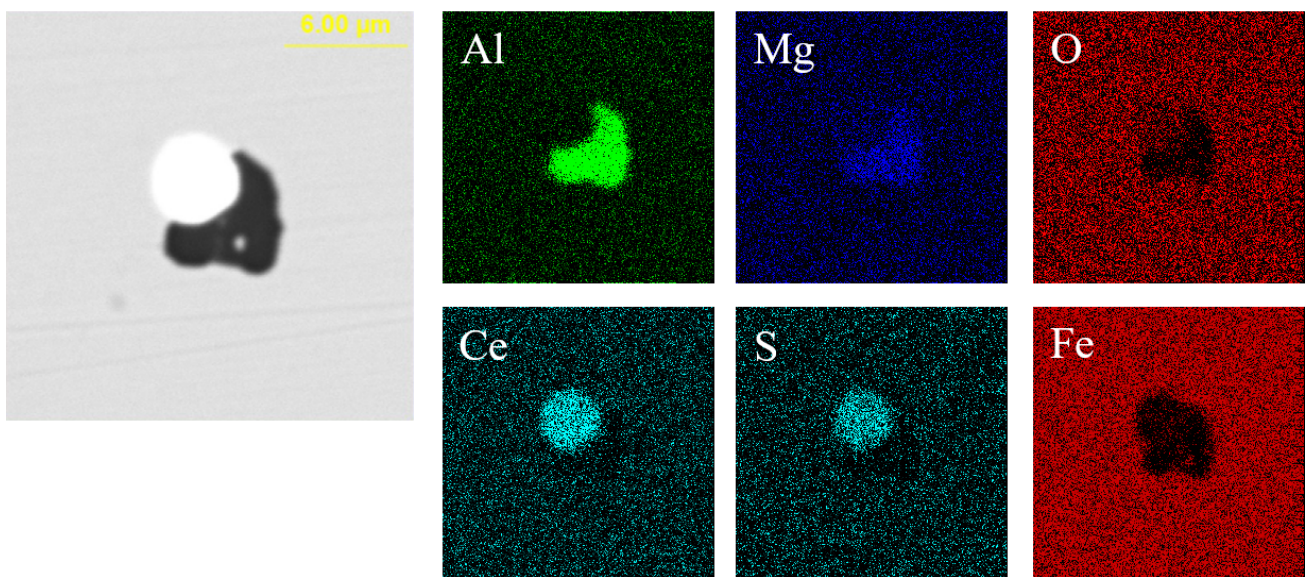
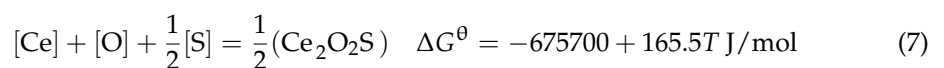
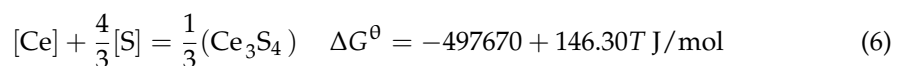
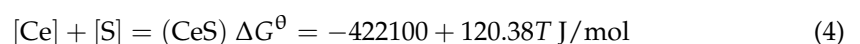
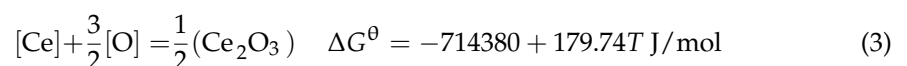
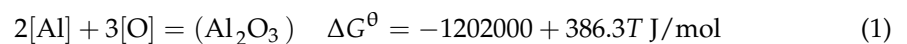


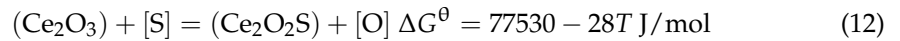
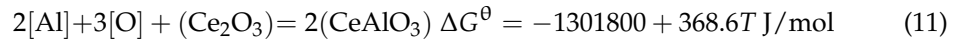
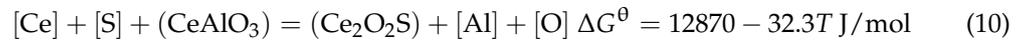
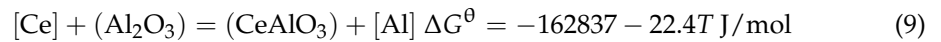
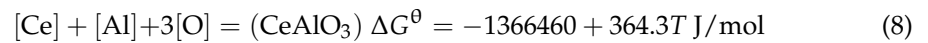
**Figure 13.** Elemental mapping of a typical inclusion in the steel with 95 ppm Ce content.

#### 4. Discussion

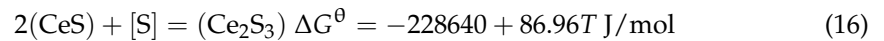
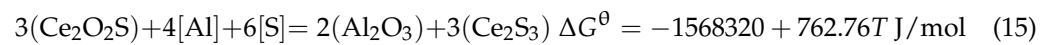
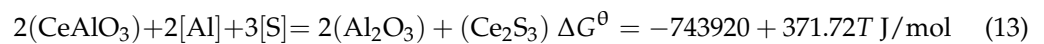
##### 4.1. Effects of Rare Earth Ce Content on Inclusion Type

The type of inclusions in W350 non-oriented silicon steel was mainly  $Al_2O_3$  without rare earth Ce. With the addition of Ce, reactions with O and S in molten steel would occur to form a variety of oxides, sulfides and oxysulfides. The possible reactions involved are as follows [20–24]:





When the rare earth Ce is fed into molten steel, it not only reacts easily with  $\text{Al}_2\text{O}_3$  to form  $\text{CeAlO}_3$ , but also converts the generated Ce-containing inclusions. The possible reactions involved are as follows:



The general expression of Gibbs free energy is:

$$\Delta G = \Delta G^\theta + RT \ln J \quad (17)$$

where  $J$  is the ratio of the activity product of the resultant and the activity product of the reactant.

Assuming that the molten steel is an ideal dilute solution, and the solute follows Henry's law, one can satisfy the following formula for calculating activity and activity coefficient [25]:

$$a_i = f_i \cdot w[i] \quad (18)$$

where  $a_i$  is the activity of component  $i$ ,  $f_i$  is the activity coefficient of component  $i$ , and  $w_{[i]}$  is the mass percentage of the element  $i$ . Thus:

$$\lg f_i = \sum_{j=1}^n e_i^j \cdot w[j] \quad (19)$$

where  $e_i^j$  is the interaction coefficient between  $j$  element and component  $i$  in molten steel. The first-order interaction coefficient of each element in molten steel is listed in Table 4 [26–28].

**Table 4.** The first-order interaction coefficient of each element in molten steel.

$e_i^j$	C	Si	Mn	P	S	Al	O	Ce	N
S	0.11	0.063	−0.026	0.029	−0.028	0.035	−0.27	−0.856	0.01
Al	0.091	0.0056	0.012	0.05	0.03	0.045	−6.6	−0.43	−0.058
O	−0.45	−0.131	−0.021	0.07	−0.133	−3.9	−0.2	−0.57	0.057
Ce	−0.077	-	0.13	1.77	−39.8	−2.25	−5.03	−0.003	-

Figure 14 shows the stability diagram of  $\text{Al}_2\text{O}_3$ - $\text{CeAlO}_3$ - $\text{Ce}_2\text{O}_2\text{S}$ - $\text{Ce}_x\text{S}_y$  in non-oriented electrical steel. Obviously, with the increase in Ce content in the steel, the evolution sequence of inclusions was  $\text{CeAlO}_3 \rightarrow \text{Ce}_2\text{O}_2\text{S} \rightarrow \text{Ce}_x\text{S}_y$ . Based on the experimental results, the types of inclusions in the steel were mainly  $\text{CeAlO}_3$ - $\text{Ce}_2\text{O}_2\text{S}$ - $(\text{AlN})$  when the Ce content was 10 ppm. When the Ce content was 14 ppm, the inclusions were composed of composite phases. The core was mainly  $\text{CeAlO}_3$ - $\text{Ce}_2\text{O}_2\text{S}$  and the outer layer was wrapped with  $\text{AlN}$ . Meanwhile, the core of some inclusions was  $\text{Ce}_x\text{S}_y$ - $\text{CeAlO}_3$ . When the Ce content was 20 ppm, the composition of inclusions was also composite phases with  $\text{CeAlO}_3$ - $\text{Ce}_2\text{O}_2\text{S}$  as the core. When the Ce content was increased to 30 ppm, the main types of inclusions in the

steel were  $\text{CeAlO}_3$ - $\text{Ce}_2\text{O}_2\text{S}$ - $\text{AlN}$ . The above results showed that the rare earth inclusions in the steel were mainly  $\text{CeAlO}_3 + \text{Ce}_2\text{O}_2\text{S}$  when the added Ce content was 10~30 ppm.

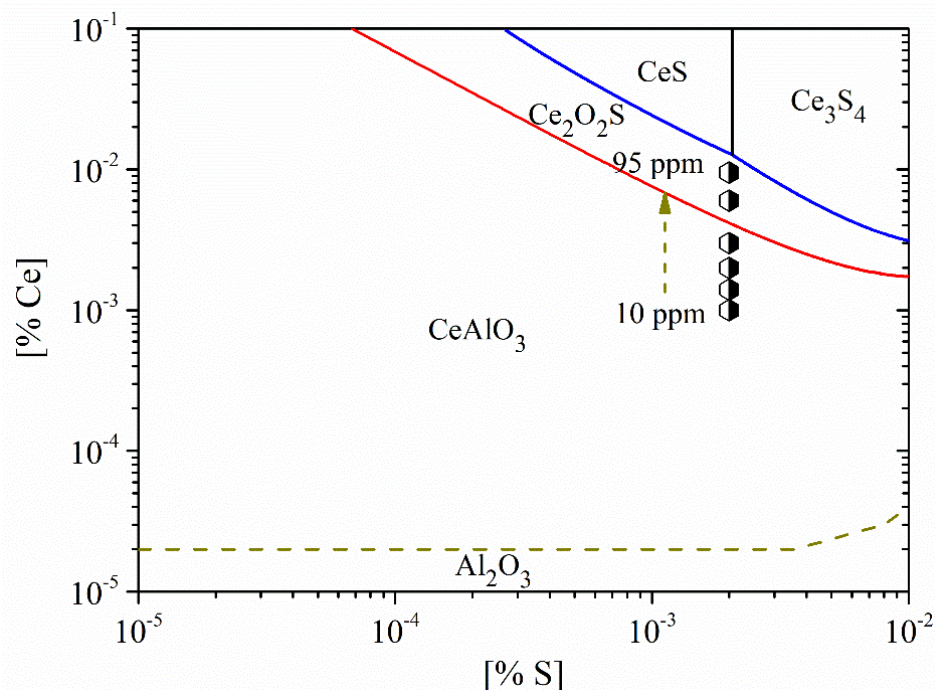


**Figure 14.** Stability diagram of  $\text{Al}_2\text{O}_3$ - $\text{CeAlO}_3$ - $\text{Ce}_2\text{O}_2\text{S}$ - $\text{Ce}_x\text{S}_y$  in non-oriented electrical steel.

Furthermore, when the Ce content was increased to 60 ppm, the composition of inclusions in the steel was mainly  $\text{Ce}_2\text{O}_2\text{S}$  and some inclusions contained a small amount of  $\text{CeAlO}_3$ . The inclusions were changed to  $\text{Ce}_x\text{S}_y$ - $\text{Ce}_2\text{O}_2\text{S}$  when the Ce content was 95 ppm. As shown in Figure 14, when the added Ce content is 95 ppm, the composition of the inclusions is located near the boundary between  $\text{Ce}_x\text{S}_y$  and  $\text{Ce}_2\text{O}_2\text{S}$ , which was consistent with the experimental results.

Figure 14 also shows that the critical Ce content for the conversion between  $\text{CeAlO}_3$  and  $\text{Ce}_2\text{O}_2\text{S}$  was 41 ppm. To ensure the inclusions transformed from  $\text{CeAlO}_3$  to  $\text{Ce}_2\text{O}_2\text{S}$ , the Ce content in the steel had to be greater than 41 ppm. Due to the addition of rare earth Ce elements, the formation of rare earth aluminates, rare earth oxygen sulfides and rare earth sulfides with high melting point can occur in molten steel. These large-sized composite inclusions can be used as heterogeneous nucleation particles and it is beneficial to control the modification and precipitation of  $\text{Al}_2\text{O}_3$ ,  $\text{MnS}$ ,  $\text{TiN}$ , and  $\text{AlN}$ , thereby improving the magnetic properties of the product.

#### 4.2. Effects of Rare Earth Ce on Size and Distribution of Inclusions

Figure 15 shows the size distribution and the average size of inclusions in steel of different heats. It shows that when the added Ce content in the steel was 10 ppm, the size of inclusions in the steel was concentrated in the range of 2.0~4.5  $\mu\text{m}$  and the corresponding proportion was 10.3~21.4%. When the added Ce content was 20 ppm and 60 ppm, the number density of inclusions in the steel was relatively low (11.11  $\#/\text{mm}^2$  and 15.14  $\#/\text{mm}^2$ , respectively). Addition of Ce decreased the amount of harmful inclusions (such as  $\text{Al}_2\text{O}_3$ ,  $\text{MnS}$ ) in the steel, which is beneficial for improving the steel cleanliness and the magnetic properties of the product. Moreover, the number density of >5.0  $\mu\text{m}$  inclusions significantly increased (6.9  $\#/\text{mm}^2$  and 6.5  $\#/\text{mm}^2$  with Ce content of 20 ppm and 60 ppm, respectively), indicating that rare earth treatment can promote the generation of large-sized inclusions in the steel. When the Ce content was 20 ppm, the average size of inclusions in the steel was at its largest, at 6.9  $\mu\text{m}$ . When the Ce content in the steel increased to 95 ppm, the number density of inclusions of all size ranges obviously increased and the total number density

was 130.1 #/mm<sup>2</sup>. It was larger than that of other Ce content levels, especially for inclusions with size range of 1.0~1.5 μm and >5.0 μm. Their number densities were 33.17 #/mm<sup>2</sup> and 33.54 #/mm<sup>2</sup>, respectively, and the corresponding proportion was about 25%, which would deteriorate the steel cleanliness and the magnetic properties of the product.

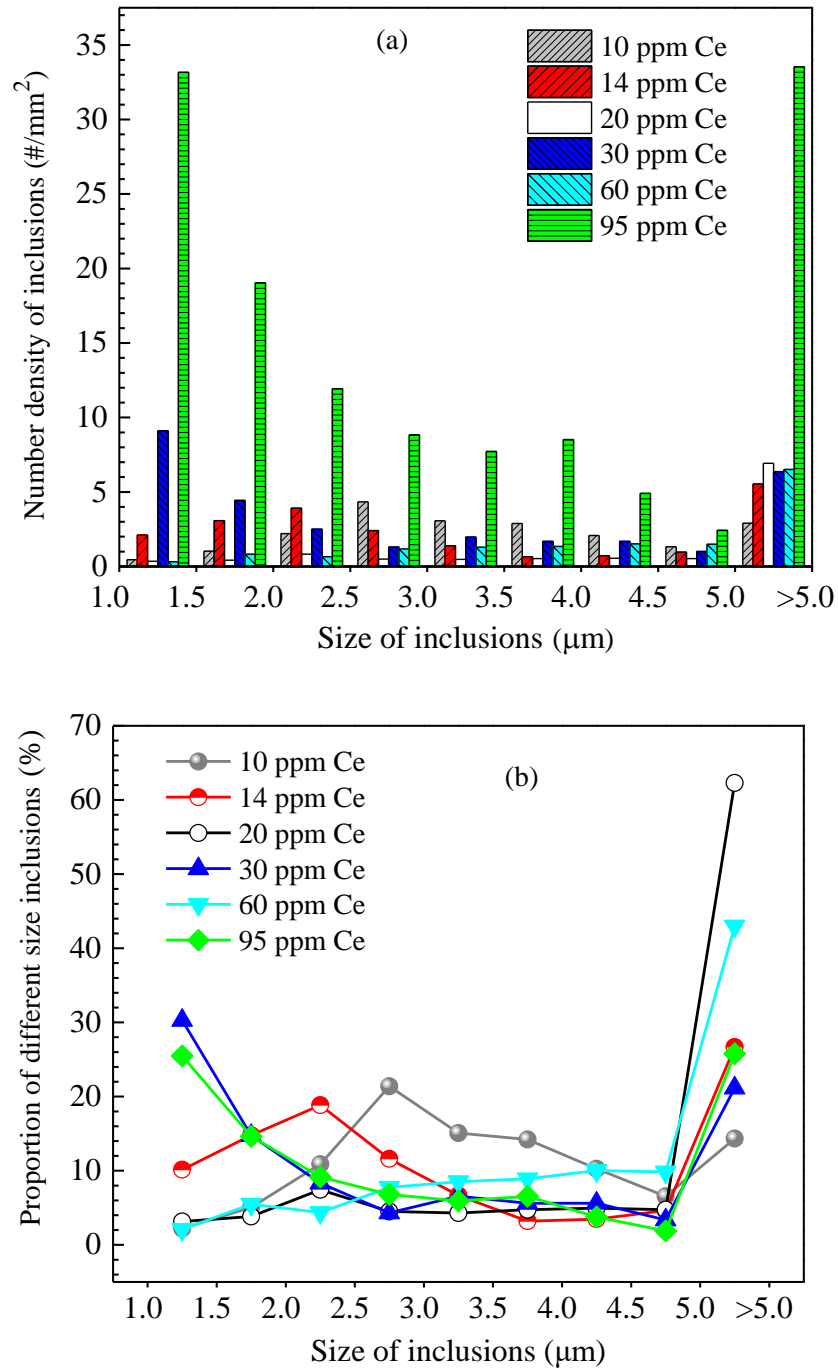
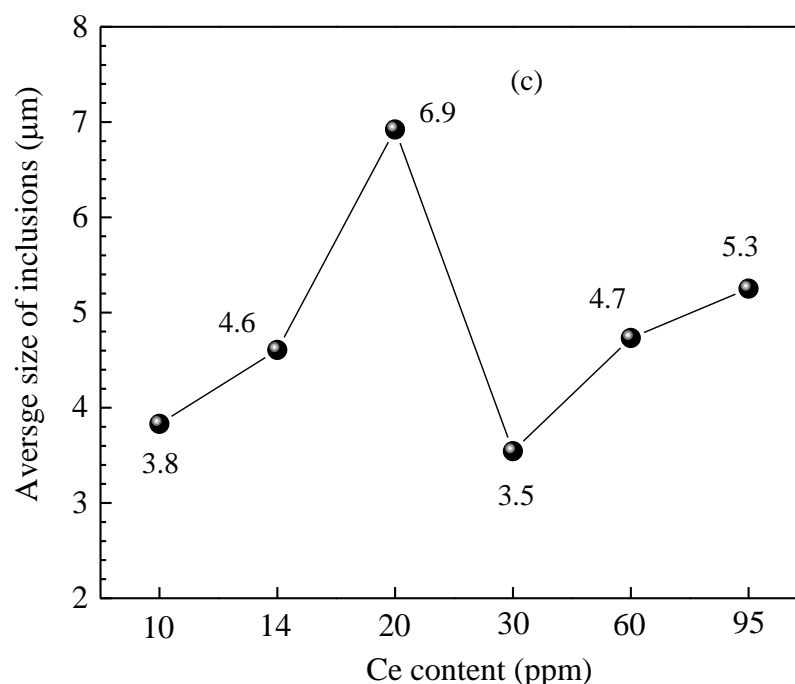


Figure 15. Cont.



**Figure 15.** Size distribution and average size of inclusions in the steel of different heats. (a) Inclusion size distribution, (b) ratio of different size inclusions, (c) average size of inclusions.

## 5. Conclusions

- (1) With the increase in the Ce content in the steel, the modification sequence of inclusions was  $\text{CeAlO}_3 \rightarrow \text{Ce}_2\text{O}_2\text{S} \rightarrow \text{Ce}_x\text{S}_y$ . When the added Ce content in the steel was 10 ppm, 14 ppm, 20 ppm and 30 ppm respectively, the rare earth inclusions were mainly  $\text{CeAlO}_3\text{-Ce}_2\text{O}_2\text{S}$ . When the added Ce content increased to 60 ppm, the rare earth inclusions were mainly  $\text{Ce}_2\text{O}_2\text{S}$  and a small amount of  $\text{CeAlO}_3$  contained in part inclusions. When the added Ce content increased continually to 95 ppm, the rare earth inclusions were mainly  $\text{Ce}_x\text{S}_y + \text{Ce}_2\text{O}_2\text{S}$ .
- (2) When the added Ce content was 95 ppm, the composition was located near the boundary between rare earth sulfide and rare earth oxysulfide. The critical Ce content for the conversion between  $\text{CeAlO}_3$  and  $\text{Ce}_2\text{O}_2\text{S}$  was 41 ppm.
- (3) The difference in the Ce content significantly affected the number density and size distribution of inclusions in the steel. When the added Ce content was 20 ppm, the number density and proportion of inclusions in the steel were lower, and its average size was larger. When the added Ce content increased to 95 ppm, the number density of inclusions in the steel significantly increased.

**Author Contributions:** Conceptualization, H.W. and H.L.; methodology, H.W.; software, H.W.; validation, H.W., Y.Z. and W.Z.; formal analysis, H.W.; investigation, H.W.; resources, H.W.; data curation, H.W., J.Q. and Y.N.; writing—original draft preparation, H.W.; writing—review and editing, H.W. and S.Q.; visualization, H.W. and H.L.; supervision, S.Q.; project administration, H.W. and S.Q.; funding acquisition, H.W. All authors have read and agreed to the published version of the manuscript.

**Funding:** This research was funded by the National Natural Science Foundation of China (Nos. 52274312 and 51804003), the Fund of Education Department of Anhui Province (Nos. 2022AH050291, 2022AH050293), the Open Project Program of Anhui Province Key Laboratory of Metallurgical Engineering & Resources Recycling (Anhui University of Technology) (No. SKF21-04), and the Jiangxi Province Major Scientific and Technological Research and Development Special Funding Project (20213AAE01009).

**Institutional Review Board Statement:** Not applicable.

**Informed Consent Statement:** Not applicable.

**Data Availability Statement:** Data available in a publicly accessible repository.

**Conflicts of Interest:** The authors declare no conflict of interest.

## References

1. Ji, S.C.; Shi, Y.H.; Zhang, F.; Lu, W.F. Review on vibration and noise of power transformer and its control measures. *High Volt. Appar.* **2019**, *55*, 1–17.
2. Yan, M.; Xiao, H.H.; Huang, X.; Zhang, Y.D. Analysis of new energy vehicles development and electrical steel demand for driving motor. *Electr. Steel* **2020**, *2*, 1–5.
3. Xu, X.X.; Qin, J.; Zhao, H.B.; Nie, J.C.; Yu, H.Y. A study on the research status and development trend of non-oriented electrical steel with high grade for new energy vehicles. *Jiangxi Metall.* **2020**, *40*, 6–11.
4. Gao, L.Y.; Zhou, H.J.; Wang, C.; Pei, R.L. Development overview and trend analysis of electric drive system of new energy vehicle. *Electr. Steel* **2020**, *2*, 27–31.
5. Chen, Z. Research on the development change and the demand of electrical steel in China in the new era. *Electr. Steel* **2019**, *1*, 1–6.
6. Guo, F.H. Study on Control of Oxide Inclusion in Non-Oriented Electrical Steel. Master's Thesis, Anhui University of Technology, Ma'anshan, China, 3 June 2019.
7. He, Z.Z.; Zhao, Y.; Luo, H.W. *Electrical Steel*; Metallurgical Industry Press: Beijing, China, 2012.
8. Zhang, X.F.; Tang, J.P.; Han, C.P.; Wang, A.L.; Zhi, J.G. Analysis on the role of rare earth in steel and the present situation of industrial production. *Chin. Rare Earths* **2020**, *42*, 117–130.
9. Dong, H.; Lian, X.T.; Hu, C.D.; Lu, H.C.; Peng, W.; Zhao, H.S.; Xu, D.X. High performance steels: The scenario of theory and technology. *Acta Metall. Sin.* **2020**, *56*, 558–582.
10. Ren, H.P.; Wu, Z.W.; Jin, Z.L. Functions and research progresses of rare earth in electrical steel. *Sci. Technol. Baotou Steel* **2018**, *44*, 1–6.
11. Wang, L.M.; Tan, Q.Y.; Li, N.; Qin, Z.; Qiu, S.T.; Gan, Y. Research progress on rare earth application technology in non-oriented electrical steels. *J. Chin. Soc. Rare Earths* **2014**, *32*, 513–533.
12. Zhang, F.; Li, G.Q.; Zhu, C.Y. Heredity characters of inclusions and electromagnetic properties of non-oriented silicon steel treated by rare earth alloy. *J. Funct. Mater.* **2013**, *44*, 1029–1033.
13. Lin, Q.; Guo, F.; Zhu, X.Y. Behaviors of La and Ce on grain boundaries in carbon manganese cleanliness steel. *J. Chin. Soc. Rare Earths* **2006**, *24*, 427–430.
14. Wang, L.M.; Du, T.; Lu, X.L.; Yue, K.X. Study of behaviors and application of micro-rare earth elements in steel. *Chin. Rare Earths* **2001**, *22*, 37–40.
15. Takashima, M.; Morito, N.; Honda, A.; Maeda, C. Non-oriented electrical steel sheet with low iron loss for high-efficiency motor cores. *IEEE Trans. Magn.* **1999**, *35*, 557–561. [[CrossRef](#)]
16. Takashima, M.; Ono, T.; Nishimura, K. Low iron loss non-oriented electrical steel for high efficiency motors “RMA Series”. *Kawasaki Steel Tech. Rep.* **1998**, *39*, 48–49.
17. Wu, C.J.; Tang, X.L. Grain boundary segregation of Ce, Mo and P and temper embrittlement of steel. *Iron Steel* **1991**, *26*, 31–35.
18. Liu, H.M.; Gao, L. The effect of rare earth metals in non-oriented silicon steel. *Iron Steel* **1987**, *22*, 41–45.
19. Yuan, Z.X.; Li, J.H.; Feng, S.J.; Wu, C.J. Grain boundary segregation of Ce and temper embrittlement of steel. *Chin. J. Eng.* **1982**, *S1*, 42–50.
20. Chen, J.X. *Manual of Chart Data for Steelmaking*; Metallurgical Industry Press: Beijing, China, 2010.
21. Itoh, H.; Hino, M.; Ban-Ya, S. Thermodynamics on the formation of spinel nonmetallic inclusion in liquid steel. *Metall. Mater. Trans. B* **1997**, *28*, 953–956. [[CrossRef](#)]
22. Vahed, A.; Kay, D.A.R. Thermodynamics of rare earths in steelmaking. *Metall. Mater. Trans. B* **1976**, *7*, 375–383. [[CrossRef](#)]
23. Li, W.C. Thermodynamics of the formation of rare-earth inclusions in steel. *Iron Steel* **1986**, *21*, 7–12.
24. Wang, L.M.; Du, T.; Lu, X.L.; Li, Z.B.; Gai, Y.C. Thermodynamics and application of rare earth elements in steel. *J. Chin. Soc. Rare Earths* **2003**, *21*, 251–254.
25. Huang, X.H. *Principles of Iron and Steel Metallurgy*; Metallurgical Industry Press: Beijing, China, 2013.
26. Zhang, L.F.; Ren, Y.; Duan, H.J.; Yang, W.; Sun, L.Y. Stability diagram of Mg-Al-O system inclusions in molten steel. *Metall. Mater. Trans. B* **2015**, *46*, 1809–1825. [[CrossRef](#)]
27. Wang, Y.; Li, C.R.; Zeng, Z.Y.; Xi, Z.B. Crystallization of alumina modified by rare earth elements in SWRS82B steel. *Iron Steel* **2020**, *55*, 69–74.
28. Pan, N.; Song, B.; Zhai, Q.J.; Wen, B. Effect of lattice disregistry on the heterogeneous nucleation catalysis of liquid steel. *J. Beijing Univ. Sci. Technol.* **2010**, *32*, 179–182.

**Disclaimer/Publisher's Note:** The statements, opinions and data contained in all publications are solely those of the individual author(s) and contributor(s) and not of MDPI and/or the editor(s). MDPI and/or the editor(s) disclaim responsibility for any injury to people or property resulting from any ideas, methods, instructions or products referred to in the content.